Progress In Electromagnetics Research, Vol. 133, 309–329, 2013

EXPERIMENTAL DEMONSTRATION OF PULSE SHAPING FOR TIME-DOMAIN MICROWAVE BREAST IMAGING

A. Santorelli[1, *], M. Chudzik[2], E. Kirshin[1], E. Porter[1], A. Lujambio[2], I. Arnedo[2], M. Popović[1], and J. Schwartz[3]

[1]Department of Electrical and Computer Engineering, McConnell Building, McGill University, 3480 University, Montreal, H3A 0E9, Canada

[2]Department of Electrical and Electronic Engineering, Public University of Navarra, Pamplona, Spain

[3]Department of Engineering Science, Trinity University, San Antonio, Texas, USA

Abstract—We experimentally demonstrate a low-cost hardware technique for synthesizing a specific electromagnetic pulse shape to improve a time-domain microwave breast imaging system. A synthesized broadband reflector (SBR) filter structure is used to reshape a generic impulse to create an ad-hoc pulse with a specifically chosen frequency spectrum that improves the detection and imaging capabilities of our experimental system. The tailored pulse shape benefits the system by improving the level of signal detection after transmission through the breast and thus permits higher-resolution images. We report on our ability to use this technique to detect the presence of tumours in realistic breast phantoms composed of varying quantities of glandular tissue. Additionally, we provide a set of images based on this experimental data that demonstrates the increased effectiveness of the system using the SBR-shaped pulse in the localisation and identification of the embedded tumour.

1. INTRODUCTION

The early detection of breast cancer is imperative to ensure the successful treatment of the disease. X-ray mammography, the

Received 10 September 2012, Accepted 18 October 2012, Scheduled 22 October 2012

* Corresponding author: Adam Santorelli (adam.santorelli@mail.mcgill.ca).

most commonly employed early-stage detection technique, has several drawbacks: it exposes patients to ionizing radiation, the exam requires the uncomfortable compression of the breast, it has difficulty imaging the breasts of young women, and it suffers from a high rate of false-positives [1]. The search for complementary imaging modalities that address these issues is of great interest. Microwave imaging techniques have shown promise as an early-stage breast cancer detection modality. The illumination of the breast with microwaves allows the presence of small tumours to be detected [2]. Several experimental systems have been previously designed in order to investigate the feasibility of the technique [3–6]. The majority of these systems [3–5] focus on frequency-domain analysis using a network analyser to record data. We have previously reported the design of an experimental system that makes use of time-domain measurements [6].

This paper focuses on the most recent hardware improvements made to the experimental system first presented in [6], and explores how these changes impact tumour detection and localisation. Using a synthesized microstrip transmission line filter we are able to reshape a generic electromagnetic impulse into a specific waveform. The benefits of this technique are two-fold: i) we are able to create a specific waveform whose time-and-frequency characteristics are optimized for the system antenna in order to maximize the useful launched power into the breast, and ii) we do so without requiring expensive GHz-band arbitrary waveform generator instrumentation, instead using an inexpensive and planar pulse-shaping filter that could be integrated onto the surface of the detection radome. Additionally, unlike our previous analyses [6, 7], in which we focused on a selected subset of antenna arrangements to demonstrate the feasibility of tumour detection using our system, we now collect data from the entire antenna array which allows us to rapidly reconstruct an image of the breast phantom. We present time-domain analysis of this newly designed experimental system, and assess its improvement on the detection and localisation of tumours in life-like tissue phantoms in comparison to the system presented in [7].

2. BACKGROUND

The illumination of the breast with electromagnetic waves in the microwave frequency band serves to identify differences in the electrical properties of the breast tissues, which are the cause of non-uniform scattering. More specifically, the reported contrast between malignant and healthy breast tissues [2] can result in a strong and detectable local scattering effect. Detection of scattered waves through the tissues is

made possible by the relatively low-loss nature of the breast tissue at microwave frequencies; hence, the recovered signals can be used for imaging purposes.

In [6] we presented an experimental time-domain system using an impulse generator to excite a wideband antenna. The pulse created from this generator was a simple, unipolar voltage impulse (-7.5 V, 70 ps half-maximum width) that was not matched to our antenna's spectral bandpassing profile and had the majority of its signal content at DC. This mismatch caused a large amount of otherwise useful transmission power to be lost right at the transmit antenna.

Rather than acquiring expensive active pulse-synthesizing hardware or employing a generic microwave bandpass filter for the antenna's basic bandwidth, we noted that recent literature [8–10] has demonstrated the possibility to design a passive, planar microwave filter with an *arbitrary* frequency response, to reshape a generic impulse into a desired target pulse. The synthesis method presented in [8] provides an exact analytical solution for converting a target frequency response into a physical profile for the dimensions of a transmission line. The synthesis technique resulted from a line of research into electromagnetic bandgap structures and is based on perturbing the physical shape of a microwave transmission line. Following the procedures developed in [8–10], and knowing *a priori* the shape of the original available impulse and the frequency response of the transmitting antenna, it is possible to determine the optimal frequency response of the microstrip line to be fabricated. We refer to this fabricated microstrip line as a synthesized broadband reflector (SBR) because the resulting filter is reflective rather than transmissive (i.e., the resulting target pulse is collected upon reflection backwards through the filter's input port).

Our purpose in choosing to use a hardware approach (as opposed to software-based programmable pulse generators) is primarily because, while the state of the technology is still in flux, integrating arbitrary pulse-synthesis in the GHz spectrum is comparatively more costly. Fabricating an SBR (nothing more than metal trace on dielectric) to passively synthesize a target waveform is much cheaper than acquiring a commercial arbitrary waveform generator in the GHz frequency range. Additionally, one can envision future microwave imaging systems that are conformal in nature in which the system is designed to adhere to the contour of the breast. The potential exists to have this pulse shaping circuitry directly integrated into the conformal measurement device by implementing the microstrip as a contour-mapped structure.

The signals detected after transmission through the breast phantom with the original (generic impulse) system were weak

in amplitude due to their inefficient matching with the antenna, resulting in detected signals close to the noise floor of the detection instrument, which made post-processing to distinguish the tumour from surrounding tissues more difficult. The goal of the modified experimental system that incorporates the SBR is to improve the tumour response by increasing the strength and coherence of the signal detected after transmission through the breast tissue by pre-shaping the transmit pulse's frequency content in a pre-established band of interest with a higher coherent time evolution (target pulse shape). Furthermore, this approach avoids the undesirable transmission of unnecessary energy in the lower frequency range, which has an impact on the maximum input power that can be safely delivered to the breast. At low frequencies (i.e., sub-GHz) the maximum amount of energy that can be safely deposited into human tissue, based on safety standards established by the IEEE, is much lower than for GHz frequencies (for example, the maximum permissible power exposure at 300 MHz is a tenth of that at 3 GHz [11]). Using a generic low-frequency input pulse places more strict safety limits on the maximum input power that we are able to use in our system.

We have previously investigated the ability of a time-domain system to detect the presence of tumours in various life-like tissue phantoms with the use of several antenna orientations [6, 7]. The analysis presented in this paper is based on the integration of a SBR within the current system design in order to improve signal transmission and tumour detection within these tissue-mimicking phantoms. This work is focused on identifying whether or not this integration of the SBR pulse-shaping system improves the system's ability to detect a difference between a healthy breast and the same breast with a tumour present.

With an antenna array consisting of twelve co-polarized antennas arranged and placed in a hemispherical radome, we are able to collect 132 signals in a multi-static radar arrangement. We contrast the ability of the system in [7] and the improved system to detect the presence of tumours in a set of breast phantoms varying from a purely adipose hemispherical tissue phantom to complex, irregularly shaped phantoms with up to 80% glandular content. We demonstrate here that our low-cost approach to pulse-shaping allows us to create a higher-resolution image of the breast phantom and improves localisation of the embedded tumour.

3. EXPERIMENTAL SYSTEM

The following section provides details regarding the individual components that make up the experimental system and is broken into four subsections. The first subsection reviews the methods the authors followed in order to create life-like breast phantoms. The second subsection provides a brief synopsis of the initial experimental system, first developed in [6], and the respective components that make up the system. We then present a characterization of the SBR device, detailing the design decisions made in the pre-fabrication process and comparing its theoretical and experimental performance. The final subsection discusses the implementation of the pulse shaping device within the microwave imaging system, the additional components required, as well as a comparison, in both the time- and frequency-domain, of the newly formed pulse with the generic impulse.

3.1. Tissue Phantoms

The breast phantoms have been constructed to realistically mimic life-like tissue. This is accomplished by creating breast phantoms with electric properties, both permittivity and conductivity, similar to those of the tissues that make up the breast anatomy. We previously outlined a procedure to create these breast phantoms from readily-available chemicals [12]. This procedure allows us to create tissue phantoms that closely mimic the various tissues composing the human breast, including skin, fat, gland, and tumour phantoms. Recently, we have adapted this methodology to create irregularly shaped breast

(a) (b)

Figure 1. An example of the heterogeneous breast phantoms. (a) A photograph of the 2-mm skin layer and the conical gland structures embedded inside the phantom. (b) An example of the realistically shaped breast phantom, exterior only.

phantoms [13], as well as modelling the glandular tissue by a discrete number of cones [14]. This creates an inhomogeneous breast phantom that closely mimics the structure of a real human breast. The glandular tissue is arranged by choosing a discrete number of cones to be embedded within the fatty tissue. An example of these recently developed phantoms is shown in Figure 1.

3.2. Initial System Description

The initial time-domain system presented in [6] uses a generic impulse generator (Picosecond Pulse Labs Impulse Generator Model 3600) to create a 70 ps full-width at half-maximum Gaussian pulse with −7.5 V amplitude. A clock (Tektronix gigaBERT 1400 generator) operating at 250 MHz is used to both drive the impulse generator (controlling the repetition rate of the input pulse) and to trigger the oscilloscope used for detection (Pico Technology PC Oscilloscope 9201). In [7] we discussed the presence of an overlap in the received signals due to consecutive pulses being too close together, thus to avoid this scenario we adjusted the clock to operate at a modest pulse repetition rate of 25 MHz.

A hemispherical dielectric of alumina (Al_2O_3), $\varepsilon_r = 9.6$, forms the radome used to provide a rigid housing structure for both the antennas and the breast phantoms. The purpose of the radome is two-fold: i) to improve antenna performance by providing better matching at the antenna launch, and ii) to ensure that the antennas are always in the same position relative to each other and the breast phantom.

The radome consists of 16 antenna slots organized into equally

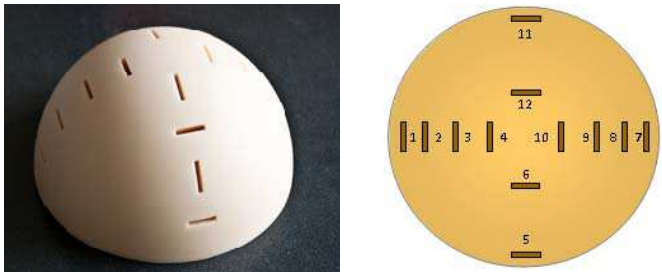

Figure 2. (a) A photograph of the fabricated radome, and (b) a simple schematic depicting the 12 co-polarized slots and their location with respect to the radome surface.

spaced quadrants (separated by 90°), each containing four slots. The radome can be thought of as a 4×4 grid. Each of the four slots in a quadrant is equally separated by 18° on an 8.5 cm radius. In two of the quadrants all four slots are oriented parallel to both each other and the open face of the radome; in the two other quadrants each alternating slot is oriented perpendicular to the previous slot. We refer to the slots that are parallel to the open face of the radome as the co-polarized slots. The slots oriented perpendicular to the co-polarized slots are referred to as being cross-polarized. In total, there are 12 co-polarized and 4 cross-polarized antenna slots. This design was chosen as initially it was uncertain whether antennas arranged in a co-polarized or cross-polarized fashion would be more useful for detection purposes. However, our early tests revealed that use of only the co-polarized responses provided the most successful tumour detection [6], thus we chose to focus solely on the co-polarized antennas. A photograph of the fabricated radome, as well as a schematic drawing of the radome with the 12 co-polarized antennas labelled, is shown in Figure 2.

The antenna used in this experimental system is a Traveling Wave Tapered and Loaded Transmission Line Antenna (TWTLTLA) [15], specifically designed for microwave imaging of the breast. It is a compact, $0.635 \times 12 \times 18\,\text{mm}^3$, wideband antenna that has been tailored for optimum performance when placed in a medium with dielectric properties similar to that of adipose breast tissue ($\varepsilon_r \approx 9$). An S_{11}

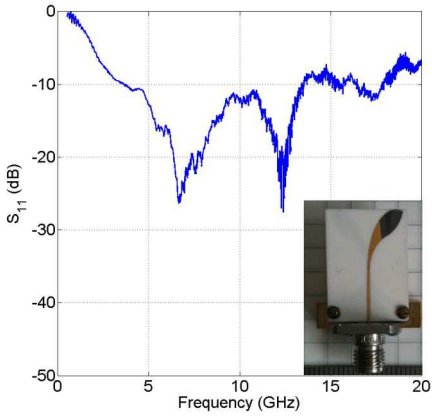

Figure 3. A plot of the S_{11} of the antenna embedded within the radome. At low frequencies the antenna is reflecting rather than transmitting much of the incident power. The inset is a photograph of the fabricated antenna.

(reflection vs. frequency) plot for the antenna embedded in the radome is presented in Figure 3 along with an inset image of the fabricated antenna. From approximately 3–12 GHz, the S_{11} of the antenna is below −10 dB, signifying that no more than 10% of the incident power will be reflected at the transmit antenna input. At frequencies below 2 GHz the antenna exhibits an S_{11} in excess of −5 dB; in this region, the antenna reflects significant power.

3.3. Pulse Shaping and the SBR Structure

We choose to implement the SBR in microstrip technology, a popular transmission line format in which a single conductor trace runs above a ground plane on a dielectric substrate [16]. The profile of the width of the conductive trace is directly related to its frequency response. Knowing the expected input to the microstrip and the desired output, the methods of [8–10] dictate the shape of the microstrip to transform the input pulse into the target.

The SBR was fabricated on a RO3010 microwave substrate ($\varepsilon_r = 10.2$). A photograph of the fabricated SBR is shown below in Figure 4. The device is compact, measuring 2.9 cm wide, 14.3 cm long, and 1.27 mm thick (excluding the 1.9 cm thick connectors used for this discrete prototype), and the secondary port of the device (right of image) is terminated with a 50 Ω broadband load to match the resistance of the conductive strip at the terminal to reduce unwanted reflections from the termination.

The SBR was designed such that the newly reshaped pulse contains most of its energy in the 2–4 GHz range. This decision was made based on a trade-off between optimized antenna performance and the lossy nature of the breast at high frequencies. At frequencies below 2 GHz, not only is the antenna generally reflective rather than transmissive ($S_{11} > -5$ dB [15]), but also the signals in these low

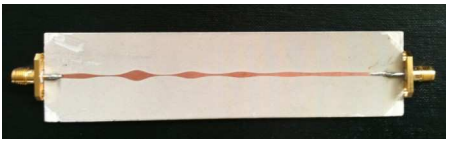

Figure 4. A photograph of the fabricated SBR structure. The dimensions of the device are 2.9 cm × 14.3 cm. The thickness of the SBR prototype is limited by the thickness of the SMA connector, however in an integrated and planar system this could be avoided by conformally placing the SBR (co-located with the antenna) on the radome.

frequencies can be detrimental to tumour detection as they undergo minimal attenuation. The reason low attenuation is a concern is that this can lead to multiple signal reflections within the breast that are picked up at the receiver, thereby clouding the received signals. Conversely, signal content at frequencies higher than 4 GHz experience too much attenuation overall as they pass through breast tissues to make discrimination from noise feasible at our detector. The 2–4 GHz range represents a "sweet spot" range between these effects.

The SBR is a reflection mode device; the input and output are at the same terminal of the device. The frequencies that make up the target pulse shape are reflected by the SBR, amplified, and launched from the antenna. A comparison plot of the target S_{11} for the desired frequency response, simulated (using Agilent ADS Momentum software), and ultimately measured from the fabricated SBR using a vector network analyser (VNA, Agilent 8703B Lightwave Component Analyzer), is shown below in Figure 5. The SBR has been designed to fully satisfy the target shown in Figure 5, keeping the main part of the energy coherently reflected in the 2–4 GHz range. From the comparison in Figure 5, the fabricated SBR performs well and is in agreement with both the target spectrum and the simulated data. The ripples that appear in the S_{11} plot for the fabricated device can be attributed to the non-ideal impedance matching that occurs at the two ports of the SBR filter; there are slight impedance differences at the connection between the VNA and the input port of the SBR, as well as the broadband 50 Ω load and the secondary port of the SBR.

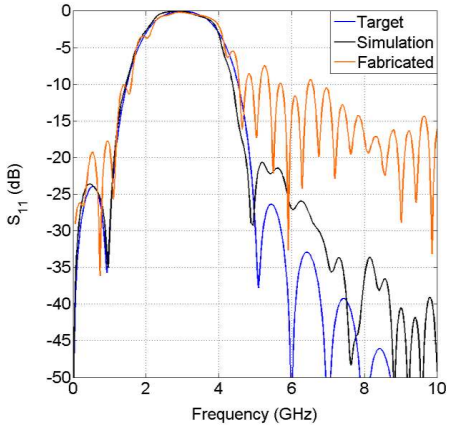

Figure 5. A comparison of the spectrum of the reflected power (S_{11}) of the SBR between the desired target spectrum, the simulation results, and the fabricated device.

3.4. System Design and Implementation

It is straightforward to analyze the effect of the presence of the SBR filter in the system. As per the system described in [6, 7] a 25 MHz clock drives the impulse generator, which creates an input impulse train. The impulse is routed to the SBR and back via a directional coupler (Pulsar CS06-09 436/9, 2–8 GHz, with 6 dB coupling loss and 0.5 dB insertion loss) and is passed to a broadband amplifier before launch. The reshaped pulse now contains only the desired spectrum; hence, we can amplify the signal before it is transmitted into the breast. Such amplification would not be as helpful with a generic impulse since we would be increasing the power only to have it reflected or lost at the transmit antenna. The amplifier (Mini-Circuits ZVE-3W-83+, 2–8 GHz operating range, +35 dB gain, max. output power 33 dBm) is used to compensate for additional losses incurred by signal transmission through the directional coupler, as well as those due to the SBR. In order to ensure that we do not exceed the power limits for linear operation of the amplifier (since our newly formed pulse has a peak power of 6 dBm), we used a broadband attenuator (−9 dB, not shown) prior to amplification. The transmitted signal scatters at various points of electromagnetic discontinuity within the breast and is collected by receiving antennas at different locations, which are then recorded for post-processing using the oscilloscope. A block diagram of the system is depicted below in Figure 6.

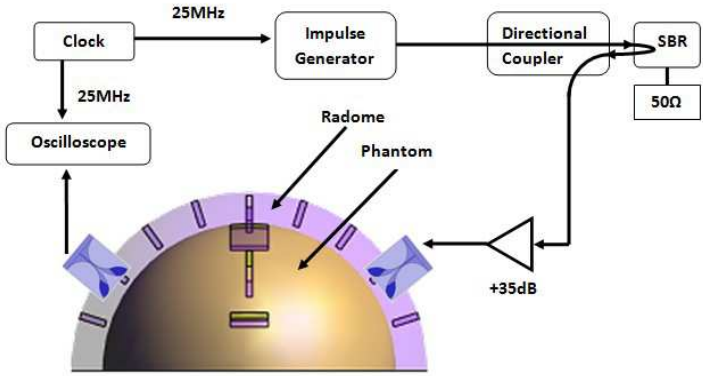

Figure 6. A high-level depiction of the complete experimental setup. The setup includes a clock to drive the pulse generator, a directional coupler to route the signal from the SBR structure towards the antenna, a radome to house the antennas and the breast phantom, and an oscilloscope to record the time-domain data.

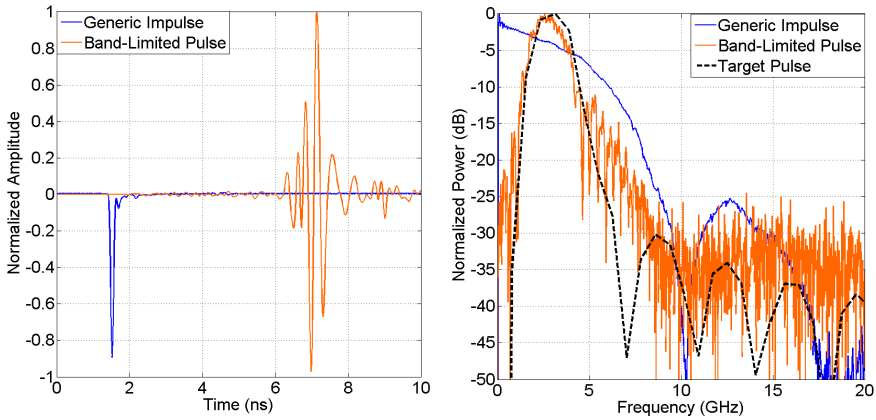

Figure 7. A comparison of the initial pulse created by the impulse generator and the newly created band-limited pulse in the both (a) the time- and (b) frequency-domain. The amplitude of the time-domain pulses have been normalized to the maximum of the reshaped pulse.

A comparison, in both the time- and frequency-domain, between the original pulse from the impulse generator and the SBR-shaped band-limited pulse is shown in Figure 7. The pulse has been transformed from a 70 ps DC-centric impulse to an AC pulse. The filtering of the DC content could have been left to the antenna, with two serious drawbacks: i) too much low-frequency content will continue to be transmitted, confounding results due to the aforementioned "multiple echoing" effects, and ii) by pre-shaping the pulse it can be subsequently and usefully amplified *before* transmitting it into the breast without exacerbating the echoing effect. In Figure 7, the amplitudes of the pulses have been normalized to the maximum of the reshaped pulse after amplification. Despite the fact that the reshaped pulse has been significantly amplified, because of insertion losses of the added SBR circuitry the peak voltage of both pulses is of the same order. There is an approximate 5 ns delay between the two pulses; this delay is due to the propagation delay from the extra cables and pulse-shaping circuitry (directional coupler, SBR, amplifier).

The majority of the power of the unshaped impulse is in the low frequency range with decreasing power as the frequency is increased. It is due to this power concentration in the low frequency range that despite poor antenna performance (at frequencies below 2 GHz) a significant portion of these unwanted frequencies are

transmitted. Figure 7 illustrates both the original and reshaped pulse spectra as generated by a Fourier transformation of their time-measured waveforms. The plot shows the suppression of the undesired frequencies outside the 2–4 GHz range.

4. METHODOLOGY

Each measurement was conducted with a pair of antennas using only one transmitting and one receiving antenna. We concentrate on antennas arranged in a co-polarized manner based on the conclusions presented in [6, 7] that demonstrated improved signal transmission and tumour detection for co-polarized antenna arrangements. Twelve antennas were placed into the co-polarized antenna slots (a labelled diagram of the location of the 12 antenna slots can be seen in Figure 2). We used a set of 8×1 co-axial switches to cycle through the 11 receiving antennas for each transmitting antenna. This allowed us to record a multi-static array of signals comprised of 132 recordings.

In order to extract the tumour response from the recorded data it is necessary to calibrate the experimental system. We made use of a differential measurement technique for calibration of time-domain systems that has been previously proposed in [17, 18]. Specifically, in [17] it was shown that using differential signals collected by comparing past and present scans provides a viable method to monitor the progress of developing tumours. This calibration procedure allowed us to remove signals arising from the effects of antenna coupling (pulse travelling directly between antennas without passing through the breast), reflections arising from the radome wall, and from the background clutter (healthy tissue). Therefore, for each measurement it was necessary to record two sets of signals. The first recording was a measurement of the "healthy" breast phantom serving as a baseline signal. The idea behind this step is that a patient would have an initial scan (or a scan at regular intervals) when they are known to be cancer-free. Future follow-up scans can then be compared to the healthy-baseline scan to simplify tumour detection. The second measurement is performed after inserting a tumour phantom into the breast phantom. Changes in the electrical properties within the breast phantoms will impact the received signals and thus an image of the breast can be produced to pinpoint the location of an embedded tumour. The use of the baseline signal as a calibration signal, as opposed to analyzing the received signals directly, allows us to easily assess the effect of the implemented hardware changes without the added complexity of imaging algorithms.

We investigated the performance of the experimental system

with and without the pulse shaping circuitry using irregularly shaped phantoms composed of 100% fat tissue, 60% glandular tissue, 70% glandular tissue, and 80% glandular tissue. This analysis is performed on raw time-domain data (without creating images) to directly assess the improvement in tumour detection due to the SBR pulse-shaping scheme. For each of the heterogeneous breast phantoms, composed of adipose and glandular tissue, a 2-mm skin layer surrounds the breast phantom. Following the procedure in [12], we created a spherical tumour phantom of 1 cm radius that was inserted into the breast phantom at a distance of 3.5 cm from the radome wall.

Following the aforementioned preliminary analysis we proceeded to contrast the two systems using reconstructed images of the breast phantoms. Using already developed imaging algorithms, we demonstrate here that use of the reshaped pulse greatly improves the localisation and identification of the tumour. In order to contrast the performance of the two systems we focus the imaging-based investigation on two homogeneous breast phantoms composed entirely of fatty tissue (one of which is irregularly shaped). We do not yet investigate heterogeneous breast phantoms using imaging techniques since our intent is primarily to verify the impact of the pulse-shaping circuitry.

5. RESULTS

We demonstrate that the use of the reshaped pulse improves the computed tumour response signal, defined as the difference between the recorded healthy baseline signal and the recorded signal when the tumour is inserted into the breast phantom. The two signals are time aligned and then subtracted from each other. In this case the healthy baseline signal serves as the ideal calibration signal; it removes both the direct pulse and the early-time response from the radome-breast interface. We make use of the computed tumour response signals in order to reconstruct an image of the breast phantom, and thus identify and localise the presence of the embedded tumour.

5.1. Time-domain Analysis

A comparison of the computed tumour response signals for the two systems is shown in Figures 8 and 9. Figure 8 corresponds to a recording made with the realistically-shaped purely adipose phantom, and Figure 9 corresponds to the data gathered from experiments with the 80% glandular content phantom. In both figures, the data corresponds to an antenna arrangement with the two antennas

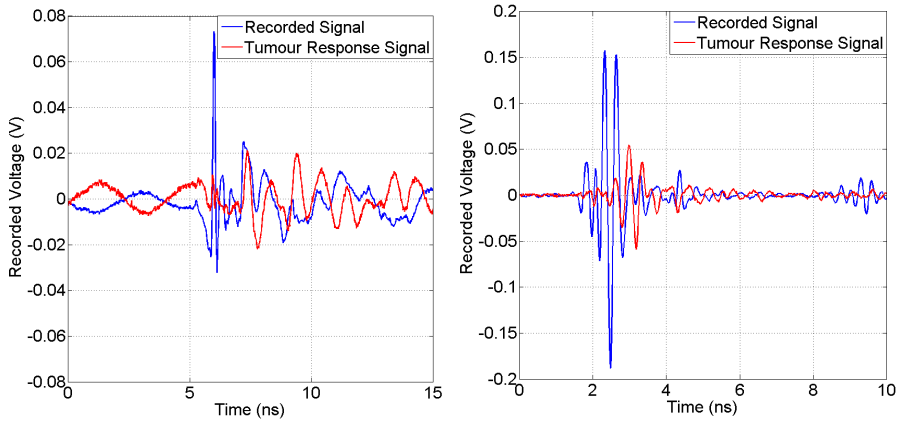

Figure 8. Time-domain comparison of the recorded signal and the tumour response signal for both (a) the original system and (b) the SBR-modified system in the realistically-shaped purely adipose breast phantom.

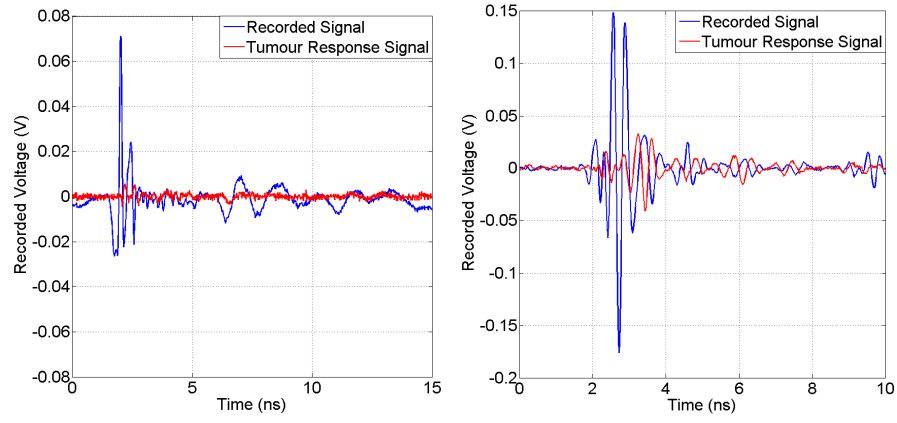

Figure 9. Time-domain comparison of the recorded signal and the tumour response signal for both (a) the original system and (b) the SBR-modified system in the realistically-shaped 80% gland breast phantom.

on the same side of the radome and stacked on top of each other (transmit antenna in slot 8, receiver in slot 9); we denote this antenna arrangement as a reflection scenario, the received signals correspond to those that have been reflected from the breast phantom and the

embedded tumour. In each figure we compare the results from using the generic and SBR-shaped pulses. Additionally, each respective plot contains two signals, i) the recorded signal representing the measurement when the tumour is embedded in the breast phantom, shown in blue, and ii) the tumour response signal (with the baseline measurement subtracted), shown in red.

The delay between the peak of the tumour response signal and the peak of the recorded measurement demonstrates that our calibration procedure is successful in removing the early-time response due to the direct pulse and the interface between the radome wall and the breast phantom. The time delay between the peak of the direct pulse and the peak of the tumour response signal can be defined as:

$$\tau = \frac{x_0\sqrt{\varepsilon}_r}{c}, \tag{1}$$

where c is the speed of light, ε_r is the relative permittivity of the breast phantom, and x_0 is the difference in the path-length travelled between the direct pulse and the signal reflecting off of the surface of the tumour. The anticipated time delay can be computed for both the purely adipose and 80% glandular phantom, using weighted-average relative permittivity values leading to $\varepsilon_r = 9$ and $\varepsilon_r = 40.4$ [19] for each respective phantom, resulting in delays of 580 ps and 1.16 ns, respectively. These delays represent theoretical minimum and maximum bounds for the tumour position and phantom compositions used here.

An additional benefit of using the SBR-shaped pulse is that the recorded signal is easily localised in time, which is in stark contrast to the signal resulting from use of the generic impulse generator (whose pulse shape has become distorted upon transmission with multiple echoes), as can be seen in Figures 8 and 9. This allows us to easily locate and identify the tumour response signal, and thus verify whether the delay between the peaks of the tumour response and the recorded signal agrees with the theoretical values.

From the plots in Figures 8 and 9, we can compute the delay between the direct pulse and the tumour response signal for the SBR-modified system to be 625 ps and 850 ps for the 100% fat and 80% gland phantom, respectively. These values fall well within the expected range of time delays, as: i) these delays are dependent on the tissues found along the path between the transmitting and the receiving antennas, and ii) phantoms are heterogeneous (all paths through an 80% gland phantom will not necessarily contain this percentage of glandular tissue). Due to the poorly defined signal shape for the original system, there is poor temporal resolution due to low frequency content which makes the signal appear to have a ringing tail, and it was impossible

Table 1. Peak tumour response comparison.

	Tumour Response [mV]		
	SBR-System	**Original-System**	**Improvement [mV]**
100% Fat	54.8	22.0	32.8
60% Gland	22.8	5.5	17.3
70% Gland	40.3	6.9	33.4
80% Gland	39.4	6.8	32.6

to obtain an accurate estimate on the time-delay between the direct pulse and the tumour response.

From Figures 8 and 9 it is evident that the use of the reshaped pulse significantly increases both the tumour response signal and the amplitude of the recorded signals. A comparison of the peak tumour response signal for each breast phantom, for each of the two experimental systems, is presented in Table 1. The use of the modified pulse leads to an increase in the tumour response signal in each of the four breast phantoms tested. The use of the SBR-modified system is especially important when attempting to detect the tumour in the highly-complex heterogeneous breast phantoms. For the 60%, 70%, and 80% glandular phantoms, the unshaped pulse has trouble detecting the tumour, as evidenced by the very weak tumour response signal; it is just above the noise floor of the system (2 mV). Using the SBR-shaped pulse, however, allows the tumour to be more easily detected in these more realistic scenarios. In all cases the peak tumour response signal occurs when the antennas are arranged in a reflection scenario.

5.2. Tumour Localisation and Identification

The Delay-and-Sum (DAS) algorithm was the first imaging algorithm applied to time-domain data for the reconstruction of an image of the breast [20]. More recently, however, the more robust Delay-Multiply-and-Sum (DMAS) image reconstruction algorithm has been reported [21]. We have applied the DMAS algorithm to the computed tumour response signals in order to produce and compare 3-D images of the interior of the two breast phantoms investigated here.

The images have been normalized to the corresponding global maximum intensity value of the reconstructed data set. This global maximum intensity value, hence forth referred to simply as the global maximum, represents the location of the most prominent EM scatterer, which should be the embedded tumour, and is denoted in the image by the '$*$' symbol. It is referred to as the global maximum since it

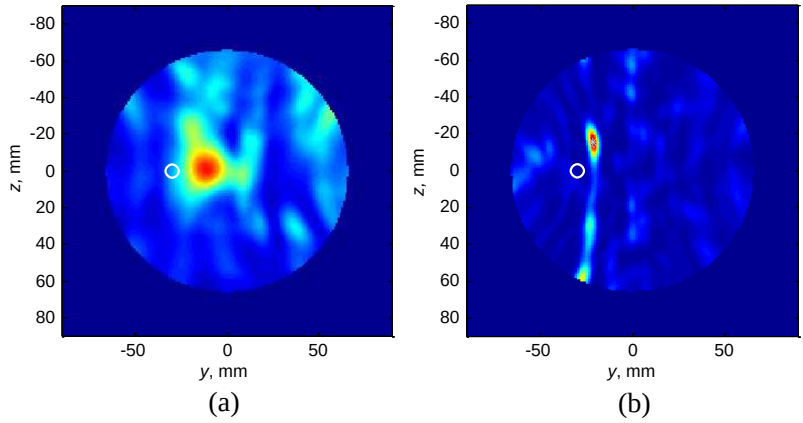

Figure 10. A coronal slice of the reconstructed 3-D image of the hemispherical adipose breast phantom comparing (a) the use of the original system and (b) the new SBR-modified system. The dark red indicates higher intensity values corresponding to stronger EM scatterers. The '$*$' denotes the global maximum and the 'o' represents the approximate tumour location based on the insertion of the tumour into the breast phantom.

represents the maximum value across the entire 3-D domain and is not simply the maximum of a single 2-D coronal slice. Within the images, dark red highlights strongly scattered electromagnetic energy, whereas blue indicates less scattering. The tumour location, based on the physical insertion of the tumour, is denoted by the '$\circ$' symbol. The reconstructed image is aligned such that the z-y plane corresponds to the plane along the chest wall and that the x-axis is oriented with the depth of the radome (corresponding to the height of the breast phantom). The centre of the image, the origin, corresponds to the centre of the radome.

A coronal slice of the reconstructed 3-D image of the hemispherical adipose breast phantom, for both the generic impulse and SBR-shaped pulse systems, is shown in Figure 10. The coronal slice is taken at the height corresponding to the centre of the embedded tumour, in this case at $x = 24.5\,\text{mm}$. From Figure 10, we are able to observe that the use of the SBR shaped pulse greatly improves the resolution of the reconstructed image, and more accurately estimates the tumour size. Furthermore, we note that in the reconstructed image using the reshaped pulse the tumour centre corresponds to the global maximum, as should be expected. In the case of the original pulse, the tumour is

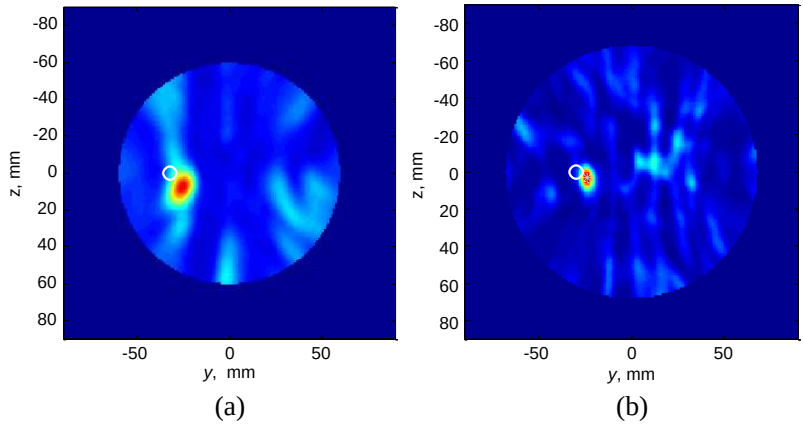

Figure 11. A coronal slice of the reconstructed 3-D image of the realistically-shaped adipose breast phantom comparing (a) the use of the original system and (b) the new SBR-modified system. The dark red indicates higher intensity values corresponding to stronger EM scatterers. The '$*$' denotes the global maximum and the '$\circ$' represents the approximate tumour location based on the insertion of the tumour into the breast phantom.

not well defined; it appears to be smoothed out over a large region in space, and additionally, unlike with the SBR-shaped pulse, the centre of the reconstructed tumour region does not correspond to the global maximum, suggesting that an artefact at a different depth (i.e., slice) not shown here is the maximum scatterer.

A similar comparison is shown in Figure 11; however, in this case the reconstructed image corresponds to the irregularly shaped adipose breast phantom. We observe that once again the use of the SBR shaped pulse greatly improves the resolution of the image by suppressing the background clutter, more accurately estimating the tumour size and location, and by correctly identifying the tumour as the maximum scatterer (as denoted by the $*$ symbol representing the global maximum of the image).

6. CONCLUSION

We have demonstrated a modified time-domain experimental system for microwave breast cancer detection using a SBR structure for pulse shaping. We are able to reshape a generic impulse from an impulse generator, using a width-modulated microstrip line, to create a pulse

with a specific frequency profile, and thus of known temporal evolution. This newly designed pulse has been chosen to optimize the performance of several components of our previous time-domain system. This system is low-cost and simple to implement and avoids the need for expensive GHz-range arbitrary pulse instrumentation.

We have demonstrated the integration of this SBR structure into our original time-domain system, and successfully tested the system's tumour detection capabilities using complex heterogeneous and life-like breast phantoms. We demonstrate that the pulse-shaping components improve the signal strength of microwaves transmitted through the breast and increase the tumour response signal. Furthermore, because the SBR-synthesized pulse is compact and of a well-known shape, it is easy to discern and localise, in time, the tumour response signal, allowing us to demonstrate that the measured delays between the peak of the direct pulse and the tumour response correspond to the estimated theoretical values.

Using an existing image reconstruction algorithm we have recreated images of two homogeneous purely adipose breast phantoms with inserted tumours. We have shown that the use of the SBR-shaped pulse significantly increases the resolution of these images, and successfully detects and localizes the tumour as the most prominent EM scatterer.

ACKNOWLEDGMENT

The authors are grateful for the funding support by the Natural Sciences and Engineering Research Council of Canada (NSERC), *le Fonds québécois de la recherche sur la nature et les technologies* (FQRNT), and *Partenariat de Recherche Orientée en Microélectronique, Photonique et Télécommunications* (PROMPT). This work has been also supported by the Spanish Ministerio de Ciencia e Innovación through the project TEC2011-28664-C02-01. M. Chudzik would like also to acknowledge Spanish Ministerio de Educación for her FPU grant. The authors would also like to thank Matthew Lee, an undergraduate student at McGill University, for all his assistance with the experimental software and phantom construction.

REFERENCES

1. Canadian Cancer Society, "What is breast cancer?" Aug. 17, 2010, Online Available: http://www.cancer.ca/.
2. Fear, E. C., P. M. Meaney, and M. A. Stuchly, "Mi-

crowaves for breast cancer detection?," *IEEE Potentials*, 12–18, Feb./Mar. 2003.

3. Klemm, M., I. J. Craddock, J. A. Leendertz, A. Preece, and R. Benjamin, "Radar-based breast cancer detection using a hemispherical antenna array — Experimental results," *IEEE Transactions on Antennas and Propagation*, Vol. 57, No. 6, 1692–1704, Jun. 2009.
4. Sill, J. M, and E. C. Fear, "Tissue sensing adaptive radar for breast cancer detection — Experimental investigation of simple tumor models," *IEEE Transactions on Microwave Theory and Techniques*, Vol. 53, No. 11, 3312–3319, Nov. 2005.
5. Xu, L., S. K. Davis, S. C. Hagness, D. W. van der Weide, and B. D. Van Veen, "Microwave imaging via space-time beamforming: Experimental investigation of tumor detection in multilayer breast phantoms," *IEEE Transactions on Microwave Theory and Techniques*, Vol. 52, No. 8, 1856–1865, Aug. 2004.
6. Porter, E., A. Santorelli, M. Coates, and M. Popović, "An experimental system for time-domain microwave breast imaging," *Proc. 5th European Conference on Antennas and Propagation (EUCAP 2011)*, Rome, Italy, Apr. 11–15, 2011.
7. Porter, E., A. Santorelli, M. Coates, and M. Popović, "Microwave breast imaging: Time-domain experiments on tissue phantoms," *Proc. 2011 IEEE International Symposium on Antennas and Propagation (AP-S 2011)*, Spokane, Washington, USA, Jul. 3–8, 2011.
8. Arnedo, I., M. A. G. Laso, F. Falcone, D. Benito, and T. Lopetegi, "A series solution for the single mode synthesis problem based on the coupled mode theory," *IEEE Transactions on Microwave Theory and Techniques*, Vol. 56, No. 2, 457–466, Feb. 2008.
9. Chudzik, M., I. Arnedo, I. Arregui, A. Lujambio, M. A. G. Laso, D. Benito, and T. Lopetegi, "Synthesis technique for microwave circuits based on inverse scattering: Efficient algorithm implementation and application," *International Journal of RF and Microwave Computer-Aided Engineering*, Vol. 21, No. 2, 163–174, 2011.
10. Arnedo, I., J. D. Schwartz, M. A. G. Laso, T. Lopetegi, D. V. Plant, and J. Azaa, "Passive microwave planar circuits for arbitrary UWB pulse shaping," *IEEE Microwave and Wireless Components Letters*, Vol. 18, No. 7, 452–454, Jul. 2008.
11. IEEE Std C95.1-1999, *IEEE Standard for Safety Levels with Respect to Human Exposure to Radio Frequency Electromagnetic Fields, 3 kHz to 300 GHz,* IEEE Press, Piscataway, NJ, 1999.

12. Porter, E., J. Fakhoury, R. Oprisor, M. Coates, and M. Popović, "Improved tissue phantoms for experimental validation of microwave breast cancer detection," *Proc. 4th European Conference on Antennas and Propagation (EUCAP 2010)*, 1–5, Apr. 12–16, 2010.
13. Porter, E., A. Santorelli, D. Coulibaly, M. Coates, and M. Popović, "Time-domain microwave breast screening system: Testing with advanced realistic breast phantoms," *Proc. 6th European Conference on Antennas and Propagation (EUCAP 2012)*, 1766–1769, Mar. 26–30, 2012.
14. Porter, E., A. Santorelli, A. Bourdon, D. Coulibaly, M. Coates, and M. Popović, "Time-domain microwave breast cancer detection: Experiments with comprehensive glandular phantoms," *2011 Asia-Pacific Microwave Conference Proceedings (APMC)*, 203–206, Dec. 5–8, 2011.
15. Kanj, H. and M. Popović, "A novel ultra-compact broadband antenna for microwave breast tumor detection," *Progress In Electromagnetics Research*, Vol. 86, 169–198, 2008.
16. Pozar, D. M., *Microwave Engineering*, 2nd Edition, Addison-Wesley, Reading, MA, 1998.
17. Byrne, D., M. O'Halloran, M. Glavin, and E. Jones, "Breast cancer detection based on differential ultrawideband microwave radar," *Progress In Electromagnetics Research M*, Vol. 20, 231–242, 2011.
18. Lai, J. C. Y., C. B. Soh, E. Gunawan, and K. S. Low, "UWB microwave imaging for breast cancer detection — Experiments with heterogeneous breast phantoms," *Progress In Electromagnetics Research M*, Vol. 16, 19–29, 2011.
19. Santorelli, A., "Breast screening with custom-shaped pulsed microwaves," Master's Thesis, Department of Electrical and Computer Engineering, McGill University, Montreal, Canada, 2012.
20. Fear, E. C., X. Li, S. Hagness, and M. Stuchly, "Confocal microwave imaging for breast cancer detection: Localization of tumors in three dimensions," *IEEE Transactions on Biomedical Engineering*, Vol. 49, 812–822, Aug. 2002.
21. Lim, H. B., N. T. T. Nhung, E. P. Li, and N. D. Thang, "Confocal microwave imaging for breast cancer detection: Delay-multiply-and-sum image reconstruction algorithm," *IEEE Transactions on Biomedical Engineering*, Vol. 55, No. 6, 1697–1704, Jun. 2008.